Spatially Resolved Investigation and Control of the Bistability in Single Crystals of the [Fe(bbpya)(NCS)$_2$] Spin Crossover Complex

Edna M. Hernández[a,b], Sipeng Zheng[c], Helena J. Shepherd[d], Dmitry S. Yufit[e], Karl Ridier[a], Salma Bedoui[f], William Nicolazzi[a], Víctor Velázquez[b], Sylvestre Bonnet[c], Gábor Molnár[a,], Azzedine Bousseksou[a,*]*

[a] Laboratoire de Chimie de Coordination, CNRS & Université de Toulouse (UPS, INPT), 205 route de Narbonne, 31077 Toulouse, France

[b] Facultad de Ciencias, Universidad Nacional Autónoma de México, Av. Universidad No 3000, 04510 Mexico City, Mexico.

[c] Leiden Institute of Chemistry, Leiden University, POB 9502, Leiden 2300, The Netherlands

[d] School of Physical Sciences, University of Kent, Park Wood Rd, Canterbury, CT2 7NH, UK

[e] Department of Chemistry, Durham University, South Road, Durham, DH1 3LE, UK

[f] Micro-Optoelectronic and Nanostructure Laboratory, Faculty of Sciences, Monastir University, Environment Avenue, 5019 Monastir, Tunisia

ABSTRACT. The spin transition in single crystals of the [Fe^{II}(bbpya)$(NCS)_2$] (bbpya = N,N-bis(2-2'-bipyrid-6-yl)amine) mononuclear complex were investigated by a combination of X-ray diffraction, Raman spectroscopy as well as optical and atomic force microscopy (AFM) methods. These studies, performed around 440 K, revealed an extremely abrupt spin transition associated with a structural phase transition from a triclinic (low spin) to a monoclinic (mixed low spin/high spin) structure. Spatially resolved observations of this transition evidenced a clear phase separation associated with heterogeneous nucleation and the formation of a moving macroscopic interface whose velocity reached in some cases 300 μms^{-1}. Using photothermal control it was possible to stabilize biphasic states of the crystal and then acquire AFM images of the phase boundary. A "saw-tooth" like topography was repeatedly observed, which most likely emerges so as to minimize the elastic strain. Remarkably, a fine spatial control of the phase boundary could be also achieved using the AFM probe itself, through probe – sample convective heat exchange.

1. Introduction

The molecular spin crossover (SCO) phenomenon has been fascinating researchers for nearly a century due to the bistability between the high spin (HS) and low spin (LS) electronic configurations.[1] Spin transition phenomena can be triggered by several external perturbations (temperature change, application of pressure, light irradiation, intense magnetic field, etc.) and entails a spectacular change in several material properties (color, magnetic properties, density, etc.). Where first-order transitions are present in SCO solids, they are accompanied by phase nucleation and domain growth with heterogeneous phase propagation. This behavior was considered from the early stages of SCO research,[2-4] but it was first explicitly demonstrated using single crystal X-ray diffraction only in 2004.[5-6] Recently, these phenomena have been studied in detail by optical microscopy in some SCO crystals[7-27] and several theoretical models[28-47] have also been proposed to describe the experimental observations.

The existing experimental methods to observe and alter the spatiotemporal development of the spin transition are based on diffraction limited far-field optical techniques, which do not have suitable spatial resolution to define the form and size of the boundary between the HS and LS phases, the minimum size of the crystal where the

phase boundary can be observed, nor the number of nuclei that are formed. For such studies *in situ*, non-invasive and high spatial resolution imaging techniques are needed. Among these, electron microscopy[48] and scanning probe microscopy[49-50] (SPM) methods have received increasing attention over the past decade. However, the use of these techniques to obtain images in the course of the SCO remain rather challenging, mainly due to the requirement of incorporating some form of external stimuli (temperature, pressure, ...) to trigger the SCO *in situ*.

Recently some of us have reported the change in the surface roughness and other topographic features of {Fe(pyrazine)[$Pt(CN)_4$]} crystals across the spin transition;[50] showing that is possible to record thermal spin transition curves with high spatial resolution using these techniques. However, further research is needed in this direction to confirm these results and generalize them to several SCO compounds. Here we present a refined picture of the microscopic details of the spin transition in $[Fe(bbpya)(NCS)]_2$ (**1**)[51] crystals using optical microscopy and AFM. This compound has a similar structure to $[Fe(bapbpy)(NCS)_2]$ **2** (bapbpy = N-(6-(6-(pyridin-2-ylamino)pyridin-2-yl)pyridin-2-yl)pyridin-2-amine), which has been extensively studied by some of us using optical microscopy and X-ray diffraction.[11, 13, 19-20, 24, 52-53] However, the transition temperature of **1** is located in a more convenient temperature range for our AFM equipment, for which cooling is technically difficult to control.

This report is organized as follows: in a first part, we report on the precise characterization of the SCO in **1** using Raman spectroscopy, optical microscopy and singe crystal X-ray diffraction at high temperatures. In particular, we evidence a stepped SCO upon heating, with a first abrupt spin transition leading to a *ca.* 50-50 % HS-LS state, followed by a very gradual spin crossover towards the HS phase. In a second part, we analyze the spatiotemporal aspects of the first, cooperative spin transition step using optical microscopy and AFM. We evidence intriguing surface undulations accompanying the phase separation and demonstrate that it is possible to control the position of the phase boundary using an AFM tip.

2. Experimental Methods

The bbpya ligand and crystals of **1** were obtained as described previously.[51]

For XRD analysis a single crystal of **1** was mounted on a glass fiber and placed into the nitrogen gas stream of an Oxford Cryosystems 700+ Cryostream open-flow cryostat at 290 K on a Bruker D8Venture diffractometer (PHOTON 100 CMOS detector, Incoatec IμS microsource, focusing mirrors, MoKα radiation, λ = 0.71073Å). After data collection at 290 K the temperature was increased by steps of 20 K and unit cell parameters were acquired at each step. At 450 K a further full dataset was collected. Subsequently the crystal was cooled to 290 K and a final dataset was collected (denoted "290 K after"). Further details regarding structure solution, refinement and unit cell dimensions as a function of *T* can be found in the Supporting Information (SI).

Variable temperature Raman spectra were acquired by means of an Xplora (Horiba) micro-spectrometer. The sample was enclosed in the chamber of a heating stage (Linkam THMS600) under dry nitrogen atmosphere. A Nd:YAG laser operating at 532 nm with 0.1 mW power was used as an excitation source. The laser beam was focused on a spot of approximately 1.2 μm via a long-working-distance objective (magnification = ×50, numerical aperture = 0.5), which also served to collect the scattered photons. The Rayleigh scattering was removed by an edge filter and the spectral resolution was set to ca. 3 cm^{-1}. The long axis of the needle shaped crystals was oriented perpendicular to the laser polarization direction to optimize the signal intensity, but no further studies of polarization effects were done.

Optical microscopy images of crystals were recorded in bright-field either in transmission or in reflectivity modes using an Olympus BX51 microscope equipped both with a color CMOS camera (IDS UI-1250ML) and a thermoelectrically cooled CCD camera (Andor Ikon-M). The sample was illuminated by a halogen lamp (400 - 700 nm), but in certain cases the spectral range was reduced using a band-pass filter (650 ± 25 nm) where the optical contrast is maximum. The sample temperature was controlled with a Linkam THMS600 heating stage, which was purged with dry nitrogen. Depending on the size of individual crystals, objectives with different magnifications (from ×5 to ×50) were used.

For AFM measurements crystals of **1** were glued to a Si substrate, which was heated using a variable temperature stage. AFM topography images in tapping mode were acquired in a nitrogen atmosphere using a Dimension Icon

(Bruker) instrument and aluminum coated Si tips (Rtespa, Bruker, resonance frequency = 300 kHz, spring constant = 40 $N \cdot m^{-1}$). The AFM probe was heated to the same temperature as the sample. Contact mode topography images were acquired using a SmartSPM (AIST-NT) instrument and Pt coated Si probes (HQ:CSC17/Al-15 MikroMasch, spring constant = 1.08 $N \cdot m^{-1}$). An oblique laser beam (λ = 633 nm) was focused on the sample surface around the AFM tip to locally heat the sample. Optical microscopy images were recorded systematically during the AFM measurements in order to determine the spin state of the crystal.

3. Results and discussion

3.1 Sample characterization

Figure 1a shows selected representative Raman spectra of a single crystal of **1** recorded at three different temperatures (413, 460 and 513 K). The spectrum at 413 K shows several peaks between 1250 and 1650 cm^{-1} corresponding to vibrational modes of the bbpya ligand and an intense peak around 2110 cm^{-1} corresponding to the CN stretching of the thiocyanate ligands. This latter mode is well-known to be particularly sensitive to the spin state of the metal ion and was used to follow the SCO in the structurally similar compound **2**.[11, 52-53] Indeed, the 460 and 513 K spectra of **1** display two peaks in this spectral region at 2070 and 2110 cm^{-1} which we can assign to the HS and LS states, respectively. Figure 1b shows the temperature dependence of the intensity ratio of the CN stretching modes of a single crystal of **1**. For comparison the $\chi_m T$ curve of a powder sample of **1** is shown in Figure 1c, where χ_m is the magnetic susceptibility and T is the temperature.[51] While closely related, the SCO behaviors of the single crystal and powder samples show significant differences. In particular, while the $\chi_m T$ curve of the powder shows a dissymmetric hysteresis cycle, a very abrupt transition is observed in the crystals around 440 K from the LS phase to a new phase. The intensity ratio of the spin state markers shown in the Raman spectroscopy data (Figure 1a) indicates that this new phase consists of ca. 50 % - 50 % HS and LS molecules. This first step is followed by a very gradual conversion to the HS state. The transformation of the crystal to the pure HS state could not be obtained because for temperatures higher than 540 K (HS fraction = 0.75) the onset of sample decomposition was clearly observed on the surface of the crystal.

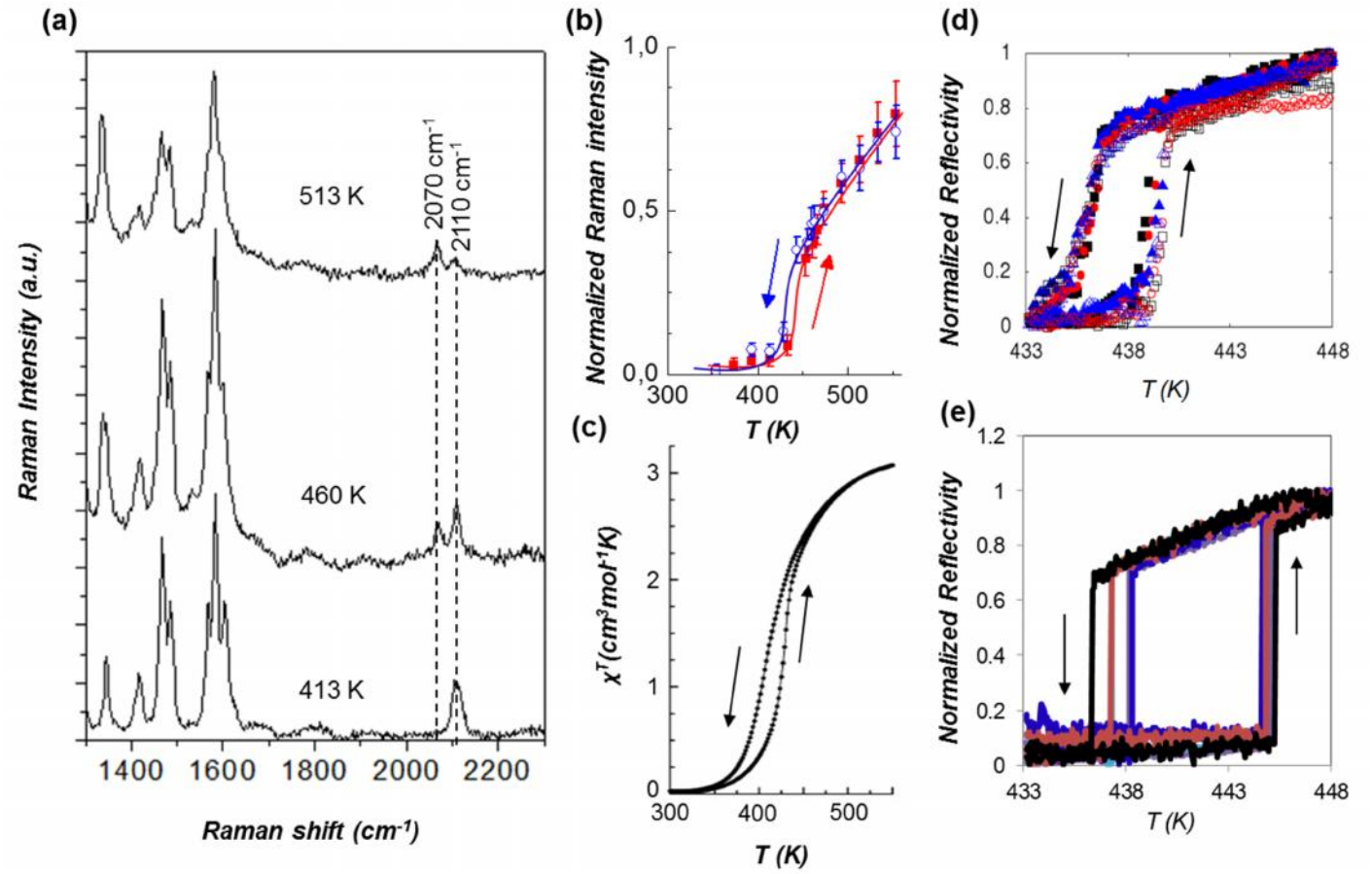

Figure 1. a) Raman spectra of a single crystal of **1** at 413, 460 and 513 K. b) Thermal variation of the normalized Raman spectral intensities [$I_{2070}/(I_{2070} + I_{2110})$]. Lines are inserted to guide the eye. Heating and cooling are indicated by arrows. c) Thermal variation of the molar magnetic susceptibility × temperature product for the powder of **1**. d) Optical reflectivity of a single crystal of **1** recorded over six successive heating-cooling cycles at two different rates. Open and closed symbols indicate 0.1 and 1 $Kmin^{-1}$, respectively. e) Optical reflectivity of another single crystal of **1** recorded over five successive heating-cooling cycles at a rate of 0.5 $Kmin^{-1}$.

The SCO in **1** is associated with significant thermochromism since the LS state exhibits higher optical densities in the visible spectral range. This property was used to follow in a more finely resolved manner the first step of the spin transition by an optical microscope. Figure 1d and 1e show two examples of optical reflectance changes as a function of the temperature. The overall shape of the transition curves is the same for the different crystals, but the fine details vary from crystal to crystal. In each case we observed a very abrupt spin transition, which was complete in less than 0.1-0.5 K. The spin transition occurs always with a hysteresis of ca. 2 - 8 K width, which is

centered in the range between 435 K and 440 K. The spin transition curves in Figure 1d were acquired for six successive thermal cycles. One can observe an abrupt increase of the reflectance around 439 K due to the transition from the LS to the mixed HS-LS phase, while the reverse transition occurs around 436 K. This crystal presents some defects that became visible after several cycles and which is reflected by the fact that the transition is not fully abrupt and the hysteresis is rather narrow. The hysteresis width is reproducible and practically heating/cooling rate independent, which confirm that it is a 'real' hysteresis, i.e. not one generated by an irreversible phenomena such as solvent loss or by a dynamic lag between the input and output (e.g. thermalization issues). For comparison, the spin transition of a higher quality crystal is depicted in Figure 1e. In this case the transition occurs in a completely discontinuous manner and it is complete in less than 0.1 K. The hysteresis in this sample is somewhat larger and centered at a higher temperature. Interestingly, the hysteresis width increases slightly between each cycle. At this point we must mention that most crystals of **1** exhibited both reversible and irreversible (i.e. self-cleavage) shape changes upon thermal cycling as well as pronounced thermosalient phenomena ('jumping crystals'[54]). Nevertheless, we succeeded in finding several robust crystals, which displayed reasonably well reproducible SCO. Perhaps not surprisingly, these crystals were usually small, thin needles.

In order to better understand the origin of the stepped nature of the spin transition the crystals were also investigated by means of high temperature X-ray diffraction. Excluding effects related to differences in temperature, the initial structure at 290 K (LS state) is comparable to that previously reported at 110 K.[51] On warming from 430 K to 450 K, the crystal undergoes a phase transition from the previously reported triclinic LS phase that has one whole molecule in the asymmetric unit, to a higher symmetry monoclinic phase containing just half a molecule in the asymmetric unit. The difference in symmetry of the molecule in the high and low temperature phases is clearly demonstrated in Figure 2a (see also Table S2 in the SI). At 450 K the molecule lies on a mirror plane (bisecting the SCN–Fe–NCS axis and N3), relating one half molecule to its symmetry equivalent. Despite the lower molecular symmetry in the low temperature phase, the FeN_6 coordination octahedron is actually more regular in this phase (see Table 1), as would be expected for the fully LS state.

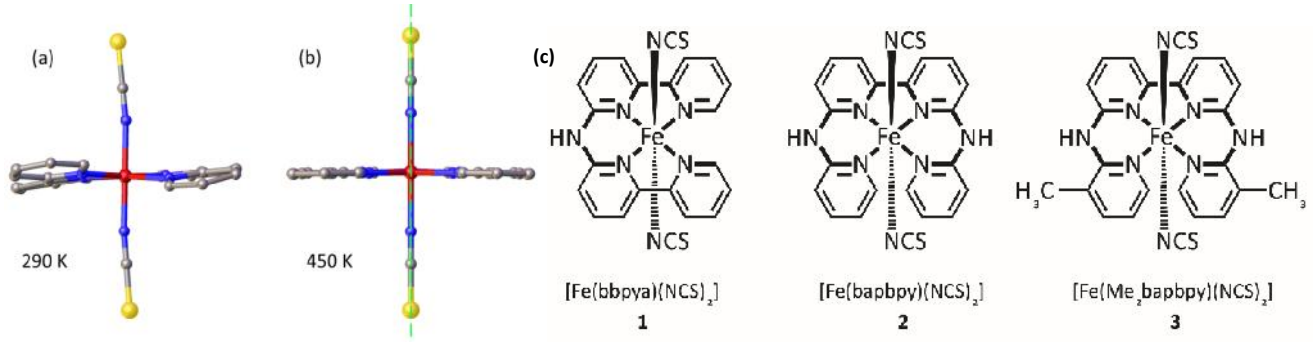

Figure 2. View down the Fe – N3 axis of the molecule in the crystal lattice at (a) 290 K and (b) 450 K indicating the significant change in symmetry between the low and high temperature phases. The green dashed line indicates the location of a mirror plane (perpendicular to the plane of view) in the high temperature phase. (c) Schematic drawings of [Fe(bbpya)$(NCS)_2$] **1,** [Fe(bapbpy)$(NCS)_2$] **2** and [Fe(Me_2bapbpy)$(NCS)_2$] **3**.

Table 1. Selected geometric parameters for the molecule of **1** at 290 K and 450 K.

	FeN_6 volume ($Å^3$)	Σ[1]
290 K (LS)[2]	9.85 (3)	47.4(13)
450 K (IP)	11.5 (1)	51.8(4)

[1]Σ is the sum of the deviation from 90° of the 12 cis N-Fe-N angles. It is equal to 0 for an ideal octahedron and increases with deformation. [2]Values obtained from the major component of the initial 290 K structure. Further details concerning treatment of disorder are given in the supporting information.

In good agreement with the Raman spectroscopy data, at 450 K the volume of the iron coordination octahedron is halfway between those expected for the pure HS (ca. 13.0 $Å^3$) and LS (ca. 10.0 $Å^3$) states (Table 1). Although the spin crossover proceeds in two steps (a first order transition followed by a gradual conversion to the high spin state), there is no evidence of more than one unique iron center at any temperature. This is significant as the observation/appearance of crystallographically distinct Fe centers in a SCO crystal lattice provides information as to the likely mechanism of SCO in the case of stepped behavior. In general, if there are multiple centers at all temperatures then there are also different chemical environments and/or intermolecular interactions at each site. Clearly this can result in stepped spin transitions as the different molecules undergo SCO at different temperatures. In other SCO materials that have only one crystallographically unique center, stepped spin crossover can result from phase transition processes, in which spontaneous structural symmetry breaking accompanies the SCO[11, 52-53, 55-59] to reveal long-range order of HS and LS states in a so-called "chessboard"

arrangement[60] in the plateau region. In the present case the XRD data reveal no evidence for long-range order of crystallographically distinct HS and LS sites, despite the presence of a crystallographic phase transition (*vide infra*). Rather, the HS and LS molecules appear to be randomly distributed throughout the lattice at 450 K. However, diffracted intensities decrease with increasing temperature, and thus it is certainly possible that long range order of HS and LS states could be present, but that the accompanying supercell reflections are too weak to be observed. Thus this issue remains unclear without further detailed investigation that is beyond the scope of the present work.

In summary for this first part of the study, what initially appeared from magnetometry to be a single-step, cooperative spin transition with dissymmetric hysteresis cycle for a macroscopic powder sample of **1**, is actually, for each individual single crystal, a combination of two distinct steps. The first step occurs around ~440 K with a small hysteresis, and is a very abrupt first-order SCO, accompanied by a crystallographic phase change, which goes from the triclinic LS, low-temperature phase to a monoclinic high-temperature phase composed of 50 % of LS and 50 % of HS molecules. Above 440 K, the second step presents as a very gradual (i.e. non-cooperative) spin crossover without phase change and towards a composition of the HT phase of 100 % of HS molecules. This theoretical fully high spin state can, however, not be reached due to the thermal decomposition of the compound (above 540 K). We must remark that, contrary to what has been reported in the literature for several other compounds, in the present case there is no plateau region between the two steps. However, the mechanism in the case of **1** is fundamentally different with respect to more commonly observed two-step spin transitions because in **1** it is a crystallographic phase transition, which gives rise to a stepped spin transition. In fact, the triclinic phase is LS at all temperatures, while the monoclinic phase exhibits a very gradual spin crossover. The stepped nature of the spin transition in **1** merely results from the fact that the temperature at which the triclinic to monoclinic crystallographic phase transition occurs coincides with the spin equilibrium temperature (i.e. ~50 % spin conversion) in the monoclinic phase. Another important remark concerns the difference between the SCO behaviors of the single crystal (Fig. 1b) and powder (Fig. 1c) samples. We attribute this difference to ensemble averaging effects in the latter consisting of crystallites with different morphologies and defects – leading to an

ensemble of different SCO curves, whose average smears out (to some extent) the intrinsic shape of the transition curve. Such differences between powder and single crystal studies have been reported in many cases (for example in compound **2** in ref. 53) and highlight the utmost importance of single crystal studies in the SCO field.

3.2 Spatiotemporal aspects of the phase transition

The spatio-temporal development of the first (abrupt) and second (gradual) steps of the spin transition in **1** were generally found to be very similar to those observed for the related compounds [Fe(bapbpy)$(NCS)_2$] (**2**)[13] and [Fe(Me_2-bapbpy)$(NCS)_2$] (**3**)[18] (see Figure 2b), respectively. As can be expected, the first, discontinuous transition is associated with formation of a nucleation point, followed by domain growth with clear phase separation. By contrast, the second, more gradual transformation occurs in a homogenous manner with a random distribution of HS and LS molecules. Selected snapshots of the nucleation and growth process associated with the first step of the spin transition for two crystals of **1** (denoted hereafter **A** and **B**), in both warming and cooling modes (1 K/min), are shown in Figure 3 and Figure S2, respectively. (See the SI for the corresponding movies.) The observations made with these crystals reveal slightly different behaviors in the spin transition process that were broadly similar to several other crystals of two different synthetic batches.

In crystal **A** (see Figure 3), the nucleation point of the high temperature (HT) phase occurs somewhere in the middle of the crystal and two well-defined straight phase boundaries are observed, propagating towards the edges of the crystal. Conversely, in the cooling mode, the nucleation of the low temperature (LT) phase occurs on both edges of the crystal (with noticeably different temperatures, ca. 441.3 K and 441.0 K for the right and left edges, respectively), and the two phase boundaries meet in the middle of the crystal. In crystal **B** (Figure S2), a single nucleation point is observed in both warming and cooling modes (on the left and the right side of the crystal for the LT and HT phases, respectively) followed by the formation of a phase boundary which travels along the entire crystal.

The spatiotemporal dynamics of the spin transition in these two crystals have been investigated for different temperature rates. Figure S3 shows the evolution of the optical transmission (at 655 ± 20 nm) of crystals **A** and

B, respectively, recorded over successive heating-cooling cycles at different temperature rates (ranging from 0.2 K/min to 4 K/min). The observed differences in the dynamic behavior of the spin transition are typically a crystal dependent feature. As crystal **A** (~ 110 × 18 × 14 μm^3) is much bigger than crystal **B** (~ 160 × 7 × 4 μm^3), it is more likely to present microstructural defects, strain or dislocations which all represent additional energy barriers to overcome. This issue is supported by the detailed investigation of the position of the phase boundary (along a line crossing the crystal **A**) as a function of time. A typical position vs. time curve is displayed in Figure S4 during the LT → HT transition shown in Figure 3. This detailed study reveals the occurrence of sudden changes of the velocity of the phase boundaries during the spin transition with successive slow-down and acceleration stages. This effect is responsible for the stepped shape of the spin transition curves displayed in Figure S3a. In crystal **A**, we find that the velocity of the HT/LT interface frontline varies from low velocity stages (typically lower than 1 μm/s) to stages during which the velocity reaches several tens of μm/s, up to ~ 88 μm/s. Velocities of the same order of magnitude are measured for all transitions realized in crystal **A**. Nevertheless, at high temperature rate (4 K/min), low velocity stages are shorter (even disappear) because it takes less time for the system to overcome energy barriers. Such slow-down and acceleration stages of the interface frontline are not observed in crystal **B**. The thorough study of the phase boundary position vs. time is more arduous in crystal **B** because the interface only appears in few images owing to its large velocity. Nevertheless, a rough estimation allows us to determine a mean velocity approximately equal to ~ 300 μm/s. Even if such spatiotemporal studies are quite scarce until now, this velocity is large compared to other spin crossover compounds reported in the literature (typically 1 – 20 μm/s).[13, 16-17, 21] This optical microscopy investigation of high-quality crystals as small as crystal **B**, reveals that the dynamics of the spin transition is intrinsically fast in this compound. In bigger crystals like crystal **A**, spin transitions are found less abrupt and involve several successive stages presumably due to the presence of defects, microstrains or dislocations. It is interesting to notice that the orientation of the phase boundary with respect to the crystal shape is a well reproducible feature in both crystals **A** and **B** (Figures 3 and S2). In all cases, we found a constant tilt angle of 46 (±1)°. As discussed by Sy et al.[22], the HT/LT interface must be oriented in a well-defined direction, which minimizes the elastic strain and the elastic energy of the system caused by the lattice mismatch between the coexisting phases. In addition, at the location of the phase boundaries a perceptible

distortion of the crystal is observed, with a reproducible angle of 177° between the edges of the different domains, likely attributable to similar effects.

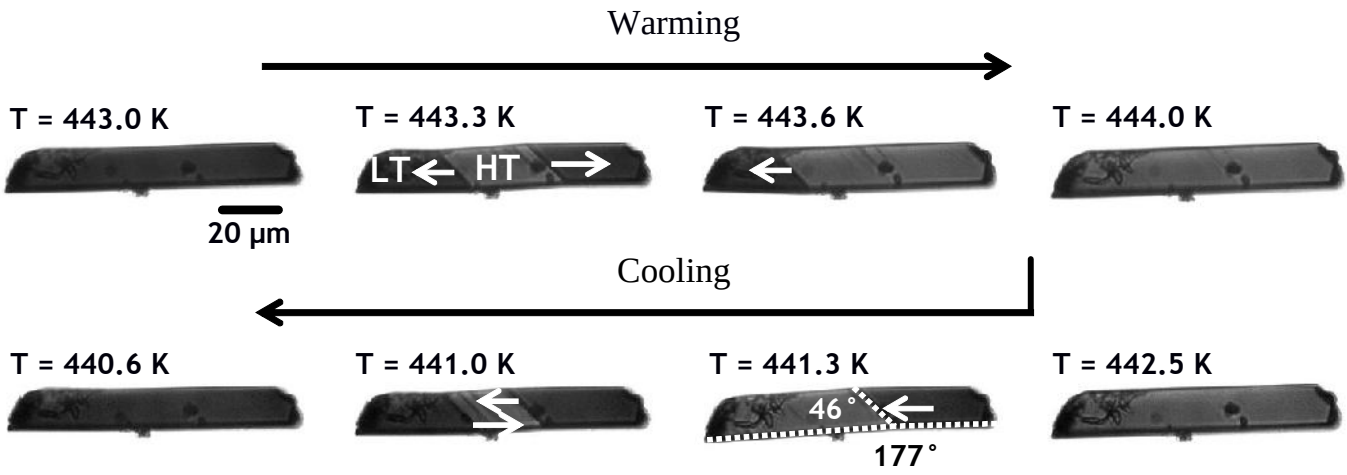

Figure 3. Optical microscopy snapshots (transmission mode at 655 ± 20 nm) of the spin transition of crystal **A** in the warming and cooling modes (1 K/min). Arrows indicate the movements of the phase boundary. The tilt angle values are also shown. See also the corresponding movie in the SI.

The spatio-temporal dynamics of the spin transition are largely determined by the properties of the phase boundary. Due to the significant lattice mismatch between the HS and LS states, elastic stress and strain are built up around the HS/LS interface.[61] The formation and propagation of the interface will be therefore governed primarily by the lattice mismatch and the elastic constants of the two phases as well as the different strain relaxation mechanisms.[62] These latter may include the formation of dislocations, microtwins, surface and composition modulations, etc.[63] Recent theoretical studies have predicted a variety of surface deformation scenarios depending on the lattice properties of the SCO material,[40] but *in-situ* experimental observations of the 3D surface morphology changes around the phase boundary have not yet been reported. To this aim we have carried out a variable-temperature AFM topography study of **1**. Crystals of **1** at room temperature revealed a relatively smooth surface with a roughness of a few nanometers. The topography is somewhat different for each crystal and depends obviously on the crystallographic orientation as well as on the growth conditions and thermal

history of the crystal (see Figure S5). As an example Figure 4 shows AFM and optical reflectivity images of a crystal of **1** acquired in the low temperature (LT) triclinic and high temperature (HT) monoclinic phases. The color change due to the spin transition is clearly observed in the photographs. The shape change of the crystal is also discernible and could even be correlated with the changes in the AFM images (see Figure S6). It is worth noting that a crack appeared on the crystal after the spin transition, which is visible both in the optical and the AFM images. Apart from this feature, however, the topography of the surface appears very similar in the two phases with clearly recognizable details in both AFM images. This contrasts with the case of {Fe(pyrazine)[Pt(CN)$_4$]} SCO crystals wherein a significant surface reconstruction was observed between the HS and LS forms.[50]

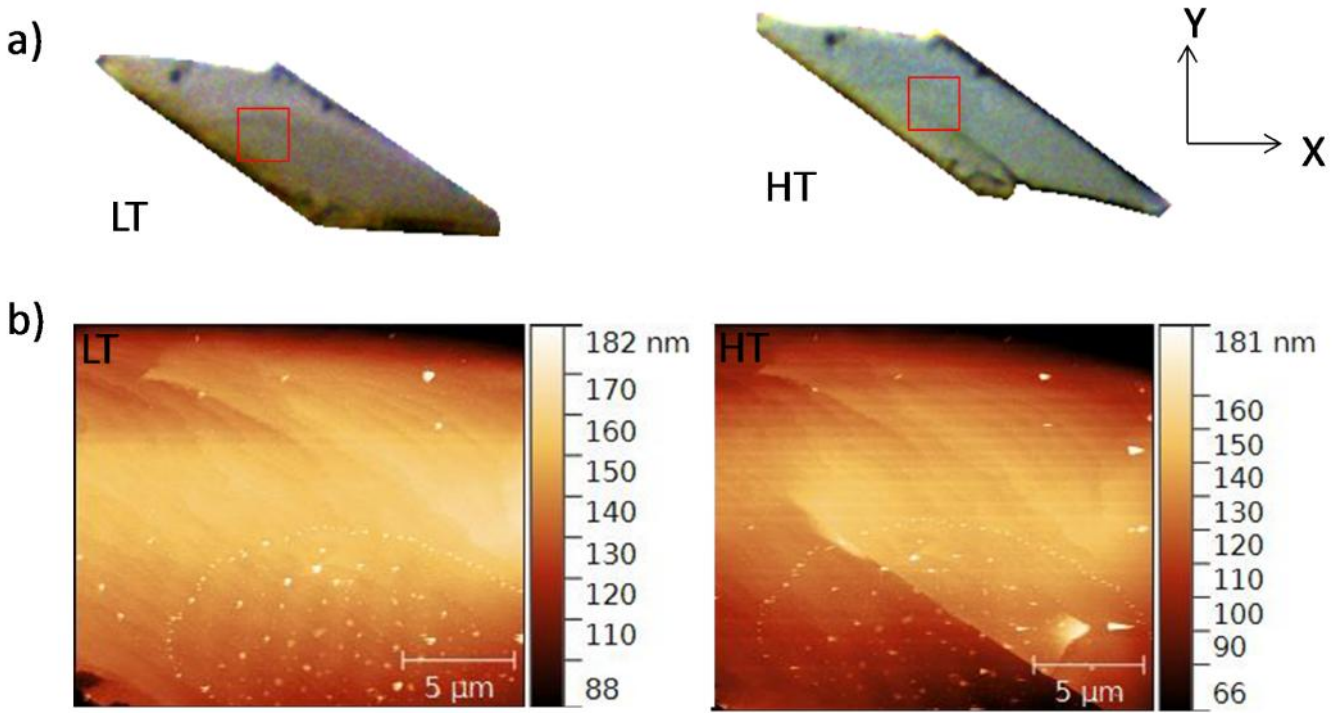

Figure 4. a) Optical and b) AFM topography images of a crystal of **1** in the high and low temperature phases. AFM topography were acquired at the area indicated by a red square in the photos.

After being thermally cycled, certain crystals presented a peculiar feature, which consisted of several nearly parallel dark lines in the optical images. An example is shown in Figure S7. AFM topography images recorded at room temperature revealed that these lines are actually nearly periodic, "sawtooth-like" topography features with

peak to peak distances of ca. 2-3 μm and peak to valley distances of ca. 50-70 nm. After a few weeks at room temperature these features disappeared and the crystal became once again flat. These topographic features are presumably related to the thermal spin transition since we observed them only after a few transition cycles. To further investigate this hypothesis we carried out a series of experiments with a crystal presenting this feature. The key enabling idea of these experiments was inspired by a recent work of Slimani et al.[21] who reported on the possibility of stabilization of biphasic (i.e. multidomain) states in a SCO crystal using photothermal effect. Selected results are shown in Figure 5 and Figure S8. Figure 5a shows two optical images of a crystal of **1** recorded at 448 K with the AFM tip engaged on the surface. At this temperature the HT phase is stable, but due to the thermal exchange with the tip, the local temperature is decreased and the crystal is partially transformed to the LT phase – as can be inferred from the optical contrast. In addition a series of alternating dark/bright lines are observed around the tip with spatial frequencies of ca. 0.1 – 0.5 μm^{-1}. We used a focused laser beam in order to locally control the temperature around the AFM tip via laser-induced heating. When the laser power was increased to 1 mW the crystal was transformed back to the HT phase and concomitantly the lines in the optical images disappeared (Figure 5a). We recorded tapping mode AFM topography images in both situations (i.e. with the laser ON and OFF), which are shown in Figure 5b together with the corresponding cross sections in Figure 5c. When the laser is turned on the topography appears very flat. On the contrary when the laser is turned off the AFM image reveals a surface undulation. The switching between these two topographies were repeated several times by turning the laser ON/OFF. We have repeated this experiment also at different locations of the same crystal and the same effects were observed (see Figure S8), the only notable difference is the eventual change of the orientation and spatial frequency of the 'accordion' lines. This change in orientation is most probably be related to the formation of cracks in the crystal while doing the experiment due to the stress and strain imposed by the temperature gradients. These experiments prove that the surface undulations in this sample are strongly related to the spin transition. As mentioned before, this latter is accompanied by a significant volume and structural change. It is plausible that the elastic strain during the transition is relaxed by the formation of these topographical features. This explanation might seem difficult to balance with the fact that in some cases the saw-tooth topography was also observed at room temperature (i.e. far from the spin transition). One may speculate that the surface

undulations are frozen-in when the sample is cooled to room temperature and this metastable structure relaxes only over a rather long period (several weeks).

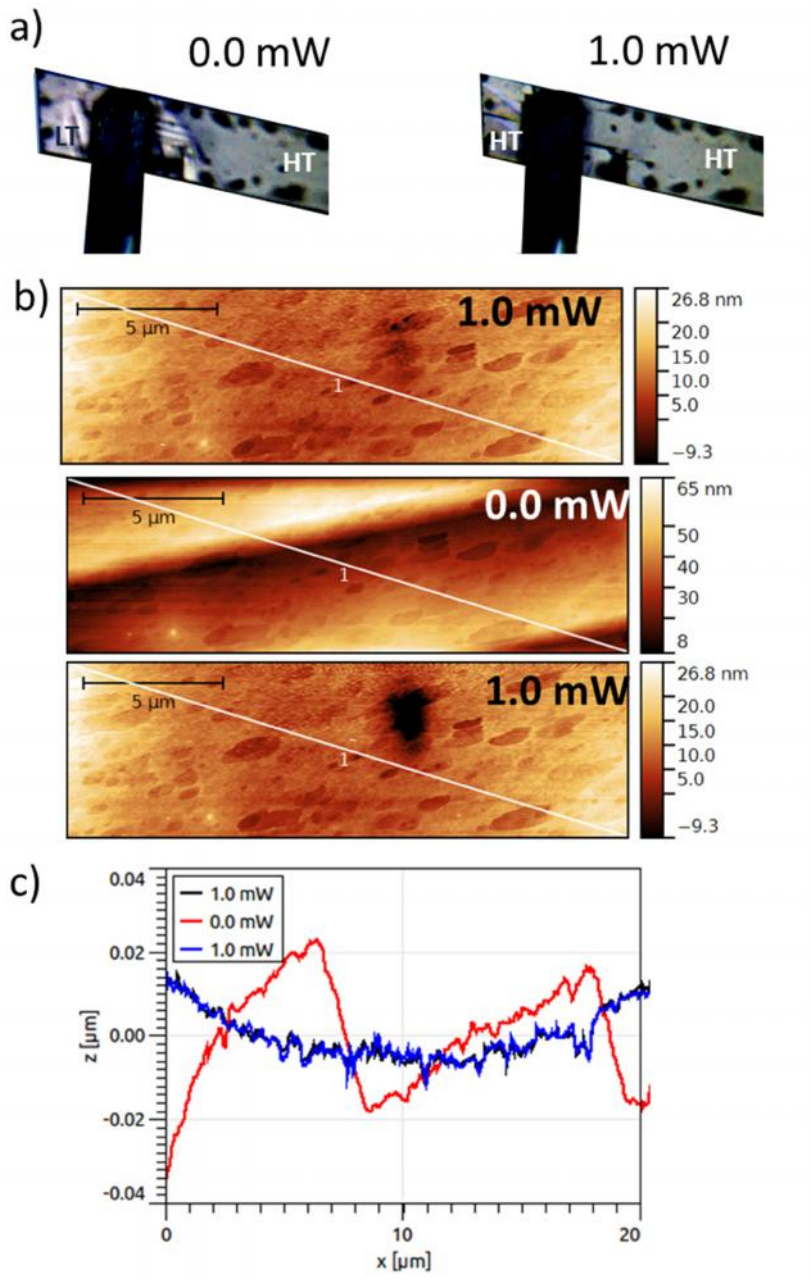

Figure 5. a) Cropped optical images (untreated images are shown in the Supporting Information), b) AFM topography images and c) topography cross-sections of a crystal of **1** recorded at 448 K with the tip engaged on the surface of the crystal. Images were acquired while turning successively on (1.0 mW) and off (0.0 mW) a laser beam (633 nm) focused near the tip.

These topographic features are also reminiscent of those observed earlier for crystals of compound **2**[13] as well as those reported in the SCO crystals $[Fe(H_4L)_2](ClO_4)_2.H_2O.2(CH_3)_2CO$ (H_4L = 2,6-bis(5-(2-hydroxyphenyl)pyrazol-3-yl)pyridine).[23] In the case of **2** these undulations were attributed to a twinning process, the LS phase being non-merohedraly twinned. Interestingly during the spin transition the formation of twin domains was also accompanied by the formation of spin domains. These latter, distinguished by Raman spectroscopy, of course, disappeared at the end of the transition. One may thus wonder if this type of surface undulation is perhaps a more general feature and should be looked for systematically in samples displaying first-order spin transitions.

During our AFM experiments we have encountered significant difficulties in controlling the spin state of the crystals due to substantial thermal exchange between the AFM tip and the sample (as well as with the sample stage). We have investigated the details of the heat exchange using a metallic nanowire thermometer and we could obtain experimental evidence that the most important contribution comes from thermal convection phenomena in our experimental conditions (see the SI for details). Due to these convection effects the probe influences the sample temperature at distances as large as a few hundred micrometers. While the probe-sample thermal exchange obviously makes for difficulties in imaging the spin transition, we recognized that at the same time it allows for a very useful way in which to manipulate and spatially control the nucleation and growth process. It was observed that by simply moving the AFM probe with respect to the sample, it is possible to induce the spin transition at different possible nucleation points and finely control the position of the phase boundary, which is very difficult or even impossible to achieve when the whole sample is heated. Figures 6 and 7 show two experiments which best illustrate this point. During these experiments the sample stage temperature was kept at 448 K. As mentioned above, at this temperature the HT phase is stable. Following sample thermalization the tip was fixed a large distance from the surface of a crystal of **1**. Then it was first moved vertically towards and away from the crystal in small steps (10 μm) and a snapshot of the sample was taken after each step. As shown in Figure 6 when the tip-sample separation was decreased to ca. 70 μm, the nucleation of the LT phase (characterized by a dark contrast) was observed in the crystal under the AFM probe. As the tip was further approached towards the crystal,

the LT domain progressively expanded towards the other end of the crystal. When the tip was finally engaged on the sample surface the LT phase progressed ca. 90 µm, which corresponds to ca. 50 % of the length of the crystal. When retracting the probe the opposite phenomenon occurs, but the approach and retract curves present a wide hysteresis of ca. 50 µm. This hysteresis obviously reflects the bistability of the sample. This experiment was reproduced three times on the same sample with the same result and it was also confirmed using other crystals. Interestingly if the tip is maintained at a certain height the phase boundary remained at the same position (for at least 2 hours). However, the elastic strain provoked irreversible damage (cracks) around the phase boundary after ca. 15-20 minutes.

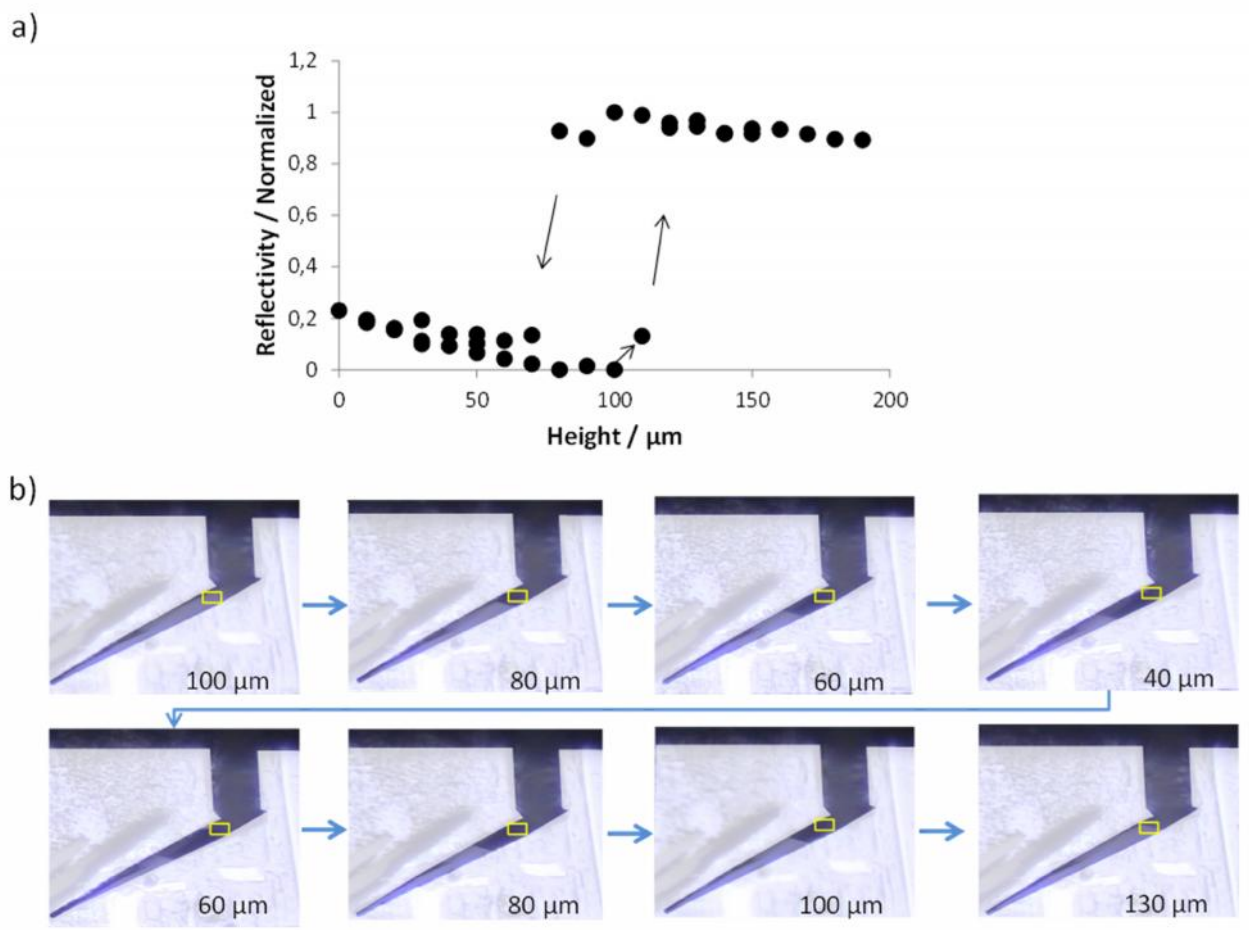

Figure 6. a) Plot of the vertical distance between the tip and the crystal surface vs. the normalized reflectance of a crystal of **1** in the area marked in the images in b). Arrows indicate increasing and decreasing tip-sample distance. A few selected images corresponding to this plot are shown in b). The tip-sample distance is indicated in each image. The experiment was performed at 448 K. The size of the images is 173 × 227 µm^2.

In a further experiment, the AFM tip was maintained at a constant height from the substrate (100 μm) and the sample stage was moved laterally parallel to the cantilever length (Figure 7). As the crystal approached the AFM probe the nucleation of the LT phase was observed at the lower end of the crystal. At this moment the distance between the AFM tip and the nucleation point was ca. 227 μm. As the tip further approached to the crystal the new phase propagated through it, i.e. the proportion of the LT phase increased. The phase boundary moved ca. 0.85 μm for every micrometer the tip approached or retracted from the crystal. The effect is perfectly reversible; as the tip is withdrawn the LT phase shrinks and finally disappears.

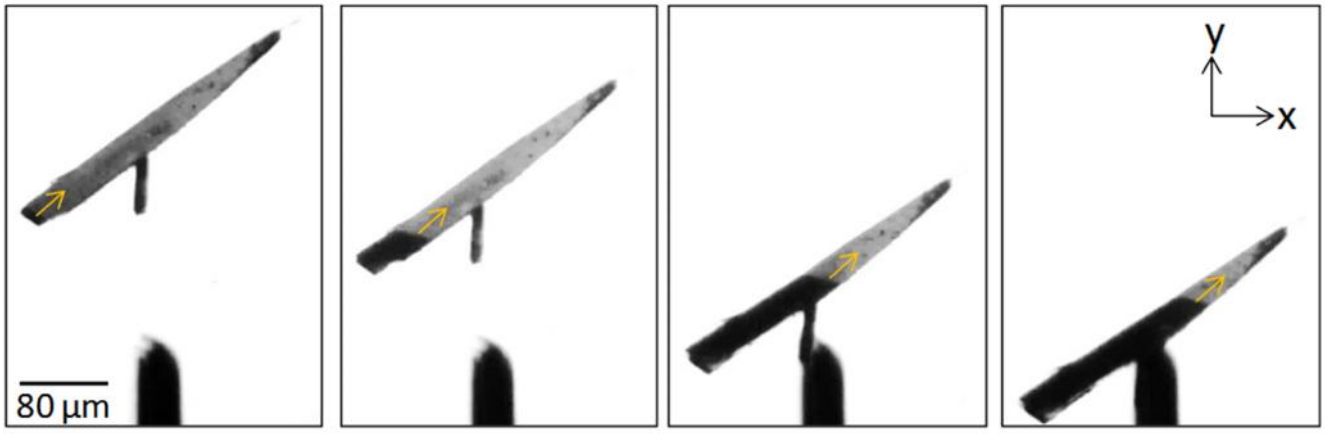

Figure 7. Optical images of a crystal of **1** while horizontally approaching an AFM probe. During the experiment the sample stage temperature (448 K) and the vertical tip - substrate distance (100 μm) were kept constant. The size of the images is 290 x 450 μm^2. (*N.B.* In the images a small crystal, attached to the crystal under study, is also visible.)

Depending on the choice of the crystal as well as on the experimental details, in particular where and how the crystal is approached by the AFM probe, we observed different behaviors, such as multiple nucleation points and thus several domains with sometimes different boundary angles and propagation directions. In general, we found that if the probe approaches the crystal far from a natural nucleation point the transition is more difficult to induce. Evidently, it is possible to force the crystal to transit in a specific point if the tip is very close to the surface and

the temperature is carefully chosen. Overall these results are conceptually somewhat similar to those reported in ref. 21 wherein light irradiation was used to finely manipulate the phase boundary in a SCO crystal. Indeed, in both cases the spatiotemporal development of the spin transition is altered by a local thermal perturbation (photothermal vs. convection). The advantage here is that the AFM tip can provide an extremely fine spatial control of the spin transition phenomena. To this aim it would be interesting to repeat these experiments in vacuum wherein convection effects are negligible and the heat transfer between the probe and the sample is dominated by conduction phenomena.

4. Conclusions

The study of single objects through local techniques such as spatial resolved Raman spectroscopy, optical microscopy and AFM are superior to bulk techniques where several objects are studied. The first can resolve details that may be veiled in the average behavior of an ensemble. Indeed, optical microscopy and Raman microspectroscopy measurements revealed that the spin transition in the $[Fe(bbpya)(NCS)]_2$ compound actually occurs in two steps, which was not observable in the case of the powder samples, where a gradual, dissymmetric transition with hysteresis was observed. In single crystals, the first step of the transition occurs between the triclinic low spin phase and a monoclinic, mixed high spin - low spin phase (ca. 50-50 %). This first step is extremely abrupt and is associated with nucleation and growth phenomena (with large velocity phase boundary), while the second step is very gradual and spatially homogenous - in analogy with the $[Fe(bapbpy)(NCS)_2]$ and $[Fe(Me_2bapbpy)(NCS)_2]$ complexes, respectively, from the same family of compounds.

Remarkably the motion of the interface between the low- and high-temperature phases can be controlled with an AFM probe. By simply moving the AFM probe with respect to the sample, we can induce the spin transition at different possible nucleation points and finely control (move forward, stop or reverse) the position of the phase boundary. Such control is very difficult or even impossible to achieve when the whole sample is heated uniformly. The effect of the AFM probe on the sample can be observed even at distances as large as 200 micrometers due to convection heat exchange phenomena. Thus, although tip-sample thermal interactions represent a serious obstacle

to acquire AFM images during the spin transition, the same phenomenon also opens up very interesting possibilities for the manipulation of the spatio-temporal dynamics of spin transition phenomena at a single crystal level. In particular, such strict control of the spatial development of the spin transition allows for increasingly fundamental studies, including the identification of the Maxwell point of the phase transition[21] or the 'mapping' of energy barriers for nucleation and growth. Despite the significant tip-sample thermal interaction it was possible to acquire AFM topography to reveal surface saw-tooth like features near the interface between the LT and HT phases. How general such undulations are in SCO materials is still an open question. Nevertheless, these features suggest that surface reconstructions, which are classical strain-relaxation phenomena in martensites for example,[63] may also happen with SCO molecular materials due to the very significant lattice mismatch between the HS and LS forms.

ASSOCIATED CONTENT

Supporting Information. Further experimental data are supplied as Supporting Information. This material is available free of charge via the Internet at http://pubs.acs.org.

AUTHOR INFORMATION

Corresponding Authors

* Email: azzedine.bousseksou@lcc-toulouse.fr, gabor.molnar@lcc-toulouse.fr

ACKNOWLEDGMENT

This work was financially supported by the LIA-LCMMC.

REFERENCES

1. *Spin Crossover in Transition Metal Compounds I-III*, Gütlich, P.; Goodwin, H. A., Eds.; in *Topics in Current Chemistry*, Springer-Verlag: Berlin Heidelberg, **2004**.
2. Sorai, M.; Seki, S. Phonon Coupled Cooperative Low-Spin $^1A_1$ High-Spin $^5T_2$ Transition in $[Fe(phen)_2(NCS)_2]$ and $[Fe(phen)_2(NCSe)_2]$ Crystals. *J. Phys. Chem. Solids* **1974**, *35*, 555–570.

3. Müller, E. W.; Spiering, H.; Gütlich, P. On the Participation of Domains in the High Spin ($^5T_2$) ⇄ Low Spin ($^1A_1$) Transition in Dithiocyanatobis (2,2′-bi-2-thiazoline) Iron (II). *J. Chem. Phys.* **1983**, 79, 1439–1443.
4. König, E.; Ritter, G.; Kulshreshtha, S. K. The Nature of Spin-State Transitions in Solid Complexes of Iron(I1) and the Interpretation of Some Associated Phenomena. *Chem. Rev.* **1985,** 85, 219-234.
5. Huby, N.; Guérin, L.; Collet, E.; Toupet, L.; Ameline, J.-C.; Cailleau, H.; Roisnel, T.; Tayagaki, T.; Tanaka, K. Photoinduced Spin Transition Probed by X-Ray Diffraction. *Phys. Rev. B* **2004**, *69*, 20101.
6. Pillet, S.; Hubsch, J.; Lecomte, C. Single Crystal Diffraction Analysis of the Thermal Spin Conversion in $[Fe(btr)_2(NCS)_2](H_2O)$: Evidence for Spin-like Domain Formation. *Eur. Phys. J. B* **2004**, *38*, 541–552.
7. Jeftic, J.; Varret, F.; Hauser, A.; Roubeau, O.; Matsarski, M.; Rivera, J.-P. Patterns During Photoexcitation and High-Spin → Low-Spin Relaxation in [Fe(ptz)6](BF4)2 Spin Transition Crystal. *Mol. Cryst. Liq. Cryst.* **1999**, *335*, 511–520.
8. Ogawa, Y.; Koshihara, S.; Koshino, K.; Ogawa, T.; Urano, C.; Takagi, H. Dynamical Aspects of the Photoinduced Phase Transition in Spin-Crossover Complexes. *Phys. Rev. Lett*. **2000,** *84*, 3181–3184.
9. Molnár, G.; Bousseksou, A.; Zwick, A.; McGarvey, J. J. The Spin-Crossover Phenomenon in the Solid State: Do Domains Play a Role? A Micro-Raman Study. *Chem. Phys. Lett.* **2003**, *367*, 593–598.
10. Goujon, A.; Varret, F.; Boukheddaden, K.; Chong, C.; Jeftić, J.; Garcia, Y.; Naik, A. D.; Ameline, J. C.; Collet, E. An Optical Microscope Study of Photo-Switching and Relaxation in Single Crystals of the Spin Transition Solid $[Fe(ptz)_6](BF_4)_2$ with Image Processing. *Inorg. Chim. Acta* **2008**, *361*, 4055–4064.
11. Bonnet, S.; Molnár, G.; Sanchez Costa, J.; Siegler, M. A.; Spek, A. L.; Bousseksou, A.; Fu, W.-T.; Gamez, P.; Reedijk, J. Influence of Sample Preparation, Temperature, Light, and Pressure on the Two-Step Spin Crossover Mononuclear Compound $[Fe(bapbpy)(NCS)_2]$. *Chem. Mater.* **2009**, *21*, 1123–1136.
12. Varret, F.; Chong, C.; Goujon, A.; Boukheddaden, K. Light-Induced Phase Separation (LIPS) in $[Fe(ptz)_6](BF_4)_2$ Spin-Crossover Single Crystals: Experimental Data Revisited through Optical Microscope Investigation. *J. Phys.: Conf. Ser.* **2009**, *148*, 12036.

13. Bedoui, S.; Molnár, G.; Bonnet, S.; Quintero, C.; Shepherd, H. J.; Nicolazzi, W.; Salmon, L.; Bousseksou, A. Raman Spectroscopic and Optical Imaging of High Spin/low Spin Domains in a Spin Crossover Complex. *Chem. Phys. Lett.* **2010**, *499*, 94–99.
14. Chong, C.; Varret, F.; Boukheddaden, K. Evolution of Self-Organized Spin Domains under Light in Single-Crystalline $[Fe(ptz)_6]$ $(BF_4)_2$. *Phys. Rev. B* **2010**, *81*, 14104.
15. Varret, F.; Slimani, A.; Boukheddaden, K.; Chong, C.; Mishra, H.; Collet, E.; Haasnoot, J.; Pillet, S. The Propagation of the Thermal Spin Transition of $[Fe(btr)_2(NCS)_2]\cdot H_2O$ Single Crystals, Observed by Optical Microscopy. *New J. Chem.* **2011**, *35*, 2333–2340.
16. Chong, C.; Slimani, A.; Varret, F.; Boukheddaden, K.; Collet, E.; Ameline, J.-C.; Bronisz, R.; Hauser, A. The Kinetics Features of a Thermal Spin Transition Characterized by Optical Microscopy on the Example of $[Fe(bbtr)_3](ClO_4)_2$ Single Crystals: Size Effect and Mechanical Instability. *Chem. Phys. Lett.* **2011**, *504*, 29–33.
17. Slimani, A.; Varret, F.; Boukheddaden, K.; Chong, C.; Mishra, H.; Haasnoot, J.; Pillet, S. Visualization and Quantitative Analysis of Spatiotemporal Behavior in a First-Order Thermal Spin Transition: A Stress-Driven Multiscale Process. *Phys. Rev. B* **2011**, *84*, 094442.
18. Arcis-Castíllo, Z.; Zheng, S.; Siegler, M. A.; Roubeau, O.; Bedoui, S.; Bonnet, S. Tuning the Transition Temperature and Cooperativity of Bapbpy-Based Mononuclear Spin-Crossover Compounds: Interplay between Molecular and Crystal Engineering. *Chem. Eur. J.* **2011**, *17*, 14826–14836.
19. Bedoui, S.; Lopes, M.; Nicolazzi, W.; Bonnet, S.; Zheng, S.; Molnár, G.; Bousseksou, A. Triggering a Phase Transition by a Spatially Localized Laser Pulse: Role of Strain. *Phys. Rev. Lett.* **2012**, *109*, 135702.
20. Bedoui, S.; Lopes, M.; Zheng, S.; Bonnet, S.; Molnár, G.; Bousseksou, A. Laser-Induced Artificial Defects (LIADs): Towards the Control of the Spatiotemporal Dynamics in Spin Transition Materials. *Adv. Mater.* **2012**, *24*, 2475–2478.
21. Slimani, A.; Varret, F.; Boukheddaden, K.; Garrot, D.; Oubouchou, H.; Kaizaki, S. Velocity of the High-Spin Low-Spin Interface Inside the Thermal Hysteresis Loop of a Spin-Crossover Crystal, via Photothermal Control of the Interface Motion. *Phys. Rev. Lett.* **2013**, *110*, 87208.

22. Sy, M.; Varret, F.; Boukheddaden, K.; Bouchez, G.; Marrot, J.; Kawata, S.; Kaizaki, S. Structure-Driven Orientation of the High-Spin–Low-Spin Interface in a Spin-Crossover Single Crystal. *Angew. Chem. Int. Ed.* **2014**, *53*, 7539–7542.
23. Craig, G. A.; Costa, J. S.; Roubeau, O.; Teat, S. J.; Shepherd, H. J.; Lopes, M.; Molnár, G.; Bousseksou, A.; Aromí, G. High-Temperature Photo-Induced Switching and Pressure-Induced Transition in a Cooperative Molecular Spin-Crossover Material. *Dalton Trans.* **2014**, *43*, 729-737.
24. Bedoui, S.; Nicolazzi, W.; Zheng, S.; Bonnet, S.; Molnár, G.; Bousseksou, A. Impact of Single Crystal Properties on Nucleation and Growth Mechanisms of a Spin Transition. *Polyhedron* **2015**, *87*, 411–416.
25. Rat, S.; Sánchez Costa, J.; Bedoui, S.; Nicolazzi, W.; Molnár, G.; Salmon, L.; Bousseksou, A. Investigation of Nucleation and Growth Phenomena during the Thermal and Light Induced Spin Transition in the $[Fe(1\text{-}bpp)_2][BF_4]_2$ Complex. *Pure Appl. Chem.* **2015**, *87*, 261–270.
26. Boukheddaden, K.; Sy, M.; Paez-Espejo, M.; Slimani, A.; Varret, F. Dynamical Control of the Spin Transition inside the Thermal Hysteresis Loop of a Spin-Crossover Single Crystal. *Phys. B* **2016**, 486, 187–191.
27. Sy, M.; Garrot, D.; Slimani, A.; Páez-Espejo, M.; Varret, F.; Boukheddaden, K. Reversible Control by Light of the High-Spin Low-Spin Elastic Interface inside the Bistable Region of a Robust Spin-Transition Single Crystal. *Angew. Chem. Int. Ed*. **2016**, *55*, 1755–1759.
28. Nishino, M.; Boukheddaden, K.; Konishi, Y.; Miyashita, S. Simple Two-Dimensional Model for the Elastic Origin of Cooperativity among Spin States of Spin-Crossover Complexes. *Phys. Rev. Lett*. **2007**, *98*, 247203.
29. Nicolazzi, W.; Pillet, S.; Lecomte, C. Two-Variable Anharmonic Model for Spin-Crossover Solids: A like-Spin Domains Interpretation. *Phys. Rev. B* **2008**, *78*, 174401.
30. Konishi, Y.; Tokoro, H.; Nishino, M.; Miyashita, S. Monte Carlo Simulation of Pressure-Induced Phase Transitions in Spin-Crossover Materials. *Phys. Rev. Lett*. **2008**, *100*, 067206.
31. Miyashita, S.; Konishi, Y.; Nishino, M.; Tokoro, H.; Rikvold, P. A. Realization of the Mean-Field Universality Class in Spin-Crossover Materials. *Phys. Rev. B* **2008**, 77, 014105.

32. Miyashita, S.; Nishino, M.; Konishi, Y.; Tokoro, H.; Boukheddaden, K.; François Varret; Rikvold, P. A. New Type of Ordering Process with Volume Change of Molecules in the Spin-Crossover Transition, and Its New Aspects of Dynamical Processes. *J. Phys.: Conf. Ser.* **2009**, *148*, 012027.
33. Enachescu, C.; Stoleriu, L.; Stancu, A.; Hauser, A. Model for Elastic Relaxation Phenomena in Finite 2D Hexagonal Molecular Lattices. *Phys. Rev. Lett.* **2009**, *102*, 257204.
34. Nicolazzi, W.; Pillet, S.; Lecomte, C. Photoinduced Phase Separation in Spin-Crossover Materials: Numerical Simulation of a Dynamic Photocrystallographic Experiment. *Phys. Rev. B* **2009**, *80*, 132102.
35. Miyashita, S.; Rikvold, P. A.; Mori, T.; Konishi, Y.; Nishino, M.; Tokoro, H. Threshold Phenomena under Photoexcitation of Spin-Crossover Materials with Cooperativity due to Elastic Interactions. *Phys. Rev. B* **2009,** *80*, 064414.
36. Chong, C.; Varret, F.; Boukheddaden, K. Evolution of Self-Organized Spin Domains under Light in Single-Crystalline $[Fe(ptz)_6](BF_4)_2$. *Phys. Rev. B* **2010**, *81*, 014104.
37. Nishino, M.; Enachescu, C.; Miyashita, S.; Boukheddaden, K.; Varret, F. Intrinsic Effects of the Boundary Condition on Switching Processes in Effective Long-Range Interactions Originating from Local Structural Change. *Phys. Rev. B* **2010**, *82*, 020409.
38. Nakada, T.; Mori, T.; Miyashita, S.; Nishino, M.; Todo, S.; Nicolazzi, W.; Rikvold, P. A. Critical Temperature and Correlation Length of an Elastic Interaction Model for Spin-Crossover Materials. *Phys. Rev. B* **2012**, *85*, 054408.
39. Nicolazzi, W.; Pillet, S. Structural Aspects of the Relaxation Process in Spin Crossover Solids: Phase Separation, Mapping of Lattice Strain, and Domain Wall Structure. *Phys. Rev. B* **2012**, *85*, 094101.
40. Boukheddaden, K.; Bailly-Reyre, A. Towards the Elastic Properties of 3D Spin-Crossover Thin Films: Evidence of Buckling Effects. *EPL* **2013**, *103*, 26005.
41. Slimani, A.; Boukheddaden, K.; Varret, F.; Nishino, M.; Miyashita, S. Properties of the Low-Spin High-Spin Interface during the Relaxation of Spin-Crossover Materials, Investigated through an Electro-Elastic Model. *J. Chem. Phys.* **2013**, *139*, 194706.

42. Slimani, A.; Boukheddaden, K.; Varret, F.; Oubouchou, H.; Nishino, M.; Miyashita, S. Microscopic Spin-Distortion Model for Switchable Molecular Solids: Spatiotemporal Study of the Deformation Field and Local Stress at the Thermal Spin Transition. *Phys. Rev. B* **2013**, *87*, 014111.
43. Nicolazzi, W.; Pavlik, J.; Bedoui, S.; Molnár, G.; Bousseksou, A. Elastic Ising-like Model for the Nucleation and Domain Formation in Spin Crossover Molecular Solids. *Eur. Phys. J. ST.* **2013**, *222*, 1137–1159.
44. Varret, F.; Paez-Espejo, M.; Boukheddaden, K. Light-Induced Instability Generated by Photo-Thermal Effect in Switchable Molecular Crystals. *EPL* **2013**, *104*, 27003.
45. Paez-Espejo, M.; Sy, M.; Varret, F.; Boukheddaden, K. Quantitative Macroscopic Treatment of the Spatiotemporal Properties of Spin Crossover Solids Based on a Reaction Diffusion Equation. *Phys. Rev. B* **2014**, *89*, 24306.
46. Slimani, A.; Boukheddaden, K.; Yamashita, K. Effect of Intermolecular Interactions on the Nucleation, Growth, and Propagation of like-Spin Domains in Spin-Crossover Materials. *Phys. Rev. B* **2015**, 92, 014111.
47. Enachescu, C.; Nishino, M.; Miyashita, S.; Boukheddaden, K.; Varret, F.; Rikvold, P. A. Shape Effects on the Cluster Spreading Process of Spin-Crossover Compounds Analyzed within an Elastic Model with Eden and Kawasaki Dynamics. *Phys. Rev. B* **2015**, *91*, 104102.
48. Van der Veen, R. M.; Kwon, O.-H.; Tissot, A.; Hauser, A.; Zewail, A. H. Single-Nanoparticle Phase Transitions Visualized by Four-Dimensional Electron Microscopy. *Nat. Chem.* **2013**, 5, 395–402.
49. Chong, C.; Berini, B.; Boukheddaden, K.; Codjovi, E.; Linarès, J.; Garcia, Y.; Naik, A. D.; Varret, F. Characterization of Spin Crossover Crystal Surface by AFM. *Phys. Stat. Sol. (a)* **2010**, *207*, 1227–1231.
50. Lopes, M.; Quintero, C. M.; Hernandez, E. M.; Velazquez, V.; Bartual-Murgui, C.; Nicolazzi, W.; Salmon, L.; Molnar, G.; Bousseksou, A. Atomic Force Microscopy and near-Field Optical Imaging of a Spin Transition. *Nanoscale* **2013**, *5*, 7762–7767.
51. Zheng, S.; Reintjens, N. R. M.; Siegler, M. A.; Roubeau, O.; Bouwman, E.; Rudavskyi, A.; Havenith, R. W. A.; Bonnet, S. Stabilization of the Low-Spin State in a Mononuclear Iron(II) Complex and High-

Temperature Cooperative Spin Crossover Mediated by Hydrogen Bonding. *Chem. Eur. J.* **2016**, *22*, 331–339.

52. Bonnet, S.; Siegler, M. A.; Costa, J. S.; Molnár, G.; Bousseksou, A.; Spek, A. L.; Gamez, P.; Reedijk, J. A Two-Step Spin Crossover Mononuclear Iron(ii) Complex with a [HS–LS–LS] Intermediate Phase. *Chem. Commun.* **2008**, *43*, 5619.
53. Shepherd, H. J.; Bonnet, S.; Guionneau, P.; Bedoui, S.; Garbarino, G.; Nicolazzi, W.; Bousseksou, A.; Molnár, G. Pressure-Induced Two-Step Spin Transition with Structural Symmetry Breaking: X-Ray Diffraction, Magnetic, and Raman Studies. *Phys. Rev. B* **2011**, *84*, 144107.
54. Skoko, Ž.; Zamir, S.; Naumov, P.; Bernstein, J. The Thermosalient Phenomenon. "Jumping Crystals" and Crystal Chemistry of the Anticholinergic Agent Oxitropium Bromide. *J. Am. Chem. Soc.* **2010**, *132*, 14191–14202.
55. Chernyshov, D.; Hostettler, M.; Törnroos, K. W.; Bürgi, H.-B. Ordering Phenomena and Phase Transitions in a Spin-Crossover Compound—Uncovering the Nature of the Intermediate Phase of [Fe(2-pic)$_3$]Cl$_2$·EtOH. *Angew. Chem. Int.Ed.* **2003**, *42*, 3825–3830.
56. Bréfuel, N.; Watanabe, H.; Toupet, L.; Come, J.; Matsumoto, N.; Collet, E.; Tanaka, K.; Tuchagues, J.-P. Concerted Spin Crossover and Symmetry Breaking Yield Three Thermally and One Light-Induced Crystallographic Phases of a Molecular Material. *Angew. Chem. Int. Ed.* **2009**, *48*, 9304–9307.
57. Bhar, K.; Khan, S.; Costa, J. S.; Ribas, J.; Roubeau, O.; Mitra, P.; Ghosh, B. K. Crystallographic Evidence for Reversible Symmetry Breaking in a Spin-Crossover d^7 Cobalt(II) Coordination Polymer. *Angew. Chem. Int. Ed.* **2012**, *51*, 2142–2145.
58. Griffin, M.; Shakespeare, S.; Shepherd, H. J.; Harding, C. J.; Létard, J.-F.; Desplanches, C.; Goeta, A. E.; Howard, J. A. K.; Powell, A. K.; Mereacre, V.; et al. A Symmetry-Breaking Spin-State Transition in Iron(III). *Angew. Chem. Int. Ed.* **2011**, *50*, 896–900.
59. Harding, D. J.; Phonsri, W.; Harding, P.; Murray, K. S.; Moubaraki, B.; Jameson, G. N. L. Abrupt Two-Step and Symmetry Breaking Spin Crossover in an iron(III) Complex: An Exceptionally Wide [LS–HS] Plateau. *Dalton Trans.* **2015**, *44*, 15079–15082.

60. Spiering, H.; Kohlhaas, T.; Romstedt, H.; Hauser, A.; Bruns-Yilmaz, C.; Kusz, J.; Gütlich, P. Correlations of the Distribution of Spin States in Spin Crossover Compounds. *Coord. Chem. Rev.* **1999**, *190*, 629–647.
61. Guionneau, P. Crystallography and spin-crossover. A view of breathing materials, *Dalton Trans.* **2014**, *43*, 382-393.
62. Spiering, H.; Boukheddaden, K.; Linares, J.; Varret, F. Total Free Energy of a Spin-Crossover Molecular System. *Phys. Rev. B* **2004**, *70*, 184106.
63. Salje, E. K. H.; Hayward, S. A.; Lee, W. T. Ferroelastic Phase Transitions: Structure and Microstructure. *Acta Cryst. A* **2005**, *61*, 3–18.

TOC graphic

High spin ↔ Low spin